Microwave Review
July 2024, Vol. 30, No. 1, pp. 37-48
DOI: 10.18485/mtts_mr.2024.30.1.6

Design of a Compact Antenna using Particle Swarm Optimization for the Entire Milli-meter Wave Range

Sneha Tiwari[1], Srikanta Pal[2]

Abstract - **Previous research in millimeter-wave antenna technology has focused on designs for specific frequency bands, such as 28 GHz, 32 GHz, 60 GHz, and 78 GHz. This paper analyzes an asymmetric dual-step antipodal petunia-shaped antenna capable of operating across the entire mm-wave frequency range from 30 GHz to 300 GHz. In the initial phase, a K-Band antenna is designed using various single radiators, including shapes such as a ball, balloon, axle, and petunia, in conjunction with a rectangular ground structure. A single radiator petunia design is enhanced to become a dual antipodal petunia radiator to achieve higher operating frequencies. This antipodal design generates multiple resonances at adjacent frequencies, resulting in broadband characteristics. To further improve performance, modifications are made to the ground structure. A novel technique inspired by radiation contouring of the antenna is proposed, which enhances impedance matching and overall antenna performance. Subsequently, a dual antipodal petunia radiator with an asymmetric step ground is optimized using the particle swarm optimization method to cover the entire millimeter-wave band (30-300 GHz). The antenna's physical dimensions are 30x30 mm², with a peak gain of 6 dBi and radiation efficiency ranging from 89% to 92% across the entire mm-wave spectrum. Notably, this proposed antenna exhibits an exceptionally low level of side lobes and excellent cross-polar discrimination, showcasing its unique design. The potential applications of this antenna span various fields, including military and imaging systems, automotive radar, telecommunications, remote sensing, security screening, and energy harvesting technology.**

Keywords – **Ant colony Optimization (ACO); Particle Swarm Optimization (PSO); Broadband Antenna; Side lobe level (SLL); Genetic Algorithm (GA); Cross-polar discrimination (XPD).**

I. INTRODUCTION

The increasing demand for energy and power highlights the critical need for alternative energy sources [1]. Millimeter-wave antennas stand out as promising candidates for energy harvesting due to their broadband characteristics. Recent research in millimeter-wave energy harvesting systems has predominantly focused on frequency bands such as 28 GHz, 38 GHz, and 60 GHz [2,3]. To achieve broadband characteristics, various optimization techniques have been employed. Different analytical optimisation methods have been applied before optimizing antenna bandwidth and radiation patterns, primarily relying on radiation-inspired optimization algorithms.

In addressing the challenges of antenna optimization, three key algorithms are commonly used: the genetic algorithm (GA), ant colony optimization (ACO), and the particle swarm optimization (PSO) algorithm. Among these, PSO optimization is renowned for its robustness in reducing antenna size, enhancing bandwidth, and achieving favorable matching properties. Given its successful track record in addressing diverse antenna design challenges, PSO is the preferred method for optimizing mathematical analysis and electromagnetic problems [4–6]. The millimeter-wave band is anticipated to offer high performance and improved data rates, making it well-suited for applications that require high data rates, precision, reliability, and artificial intelligence integration. Traditional antenna designs are inadequate for meeting the demanding requirements of millimeter-wave applications. Consequently, on-chip antenna designs utilizing metamaterials or metasurfaces have gained prominence for delivering high antenna performance with broadband characteristics [7,8]. Such designs exhibit enhanced impedance matching and radiation characteristics. In the sub-THz band, Graphene-based antennas with substrate-integrated waveguides (SIW) are employed to suppress mutual coupling in the near field and reduce surface wave propagation. Sub-wavelength slots are often incorporated on the patch to improve impedance matching and overall performance, although fabricating such designs can be challenging. In contemporary wireless transmission systems, millimeter-wave technologies are emerging as a solution for high-data-rate communications [9,10]. Millimeter-wave communication systems rely on broadband antennas with high gain characteristics to facilitate high-speed data communication and compensate for path loss between transmitters and receivers. The short wavelengths associated with mm-wave frequencies enable high spatial processing gains, allowing for theoretically incorporating numerous antenna elements to offset isotropic path loss. However, millimeter-wave communication faces challenges related to atmospheric absorption and propagation loss due to its high frequency, resulting in limited transmission distances. To address this issue, high-powered transmitters, high-gain antennas, and sensitive receivers are deployed to extend the system's communication range [11–13]. Considering the cost and durability factors of millimeter-wave communication systems, adopting a single antenna with high bandwidth and substantial gain proves to be a cost-effective approach to enhancing wireless communication systems. [14].

Research Gap: The research is continuously evolving in the field of antenna and communication, and thus, research areas show potential gaps related to antipodal antennas. The

Article history: Received July 23, 2023; Accepted January 15, 2024.

[1]Sneha Tiwari is a Ph.D. scholar, and [2]Srikanta Pal is a Professor in the Department of Electronics & Communications Engineering, BIT Mesra, Ranchi-835215, Jharkhand, India. E-mail: snehasandilya14@gmail.com

research gap in antenna design is the limited availability of compact, efficient, and broadband antennas suitable for modern wireless communication systems. While traditional antenna designs exist, they often struggle to meet the demands of emerging technologies such as 5G, IoT, and satellite communication. These systems require antennas that provide high performance across multiple frequency bands while minimizing size and complexity. The research gap is specifically in finding a solution that fulfils these requirements. Antipodal antennas are known for their broad bandwidth characteristics. However, there may be opportunities to further enhance their bandwidth performance, especially in specific frequency bands or for certain applications. Designing antipodal antennas that operate efficiently across multiple frequency bands or extremely wide frequency ranges is an ongoing challenge. Research may focus on improving their performance in these scenarios. The length (suppose L_1) of an antipodal antenna plays a crucial role in enhancing bandwidth, as it directly influences the resonant frequency and, consequently, the operational frequency range of the antenna. In antenna design, achieving a broad bandwidth is essential for accommodating a wide range of frequencies and ensuring effective communication or signal reception. While antipodal antennas are known for their simplicity, achieving high radiation efficiency across all operating frequencies remains challenging. Research can explore novel designs and materials to improve efficiency. Antennas often must be integrated with other components or structures in modern communication systems. Research may focus on developing techniques for seamless integration with minimal interference. Designing antipodal antennas that perform optimally in specific environments, such as underwater or in harsh industrial conditions, could be a valuable research direction. Research into antipodal antennas as energy harvesters, especially for low-power applications like IoT devices, can be an essential area to explore. Investigating antipodal antennas in radar and imaging applications, where factors like beamforming, resolution, and signal processing play crucial roles, could be a research focus. Research on multi-element antipodal antennas for advanced functions like MIMO (Multiple-Input, Multiple-Output) communication systems can be beneficial. A critical research aspect is Ensuring that antipodal antennas perform under various environmental conditions and mechanical stresses [15-18].

Objective- Many antipodal antennas work in lower or higher bands, but no antenna works for the entire millimeter wave band. The main objective is to design an antenna that covers a complete range of millimeter wave frequencies, i.e., from 30 GHz to 300 GHz.

Advantage- Antipodal millimeter wave antennas offer several advantages for specific applications, especially in high-frequency and high-data-rate wireless communication systems, radar systems, and imaging applications. Here are some of the benefits of antipodal millimeter wave antennas [19-21]:

1. Broadband Operation: Antipodal antennas are inherently broadband, so they can efficiently operate over a wide frequency range within the millimeter-wave spectrum. This makes them versatile for various applications that require different frequency bands.
2. Compact Size: Antipodal antennas can be designed to be compact, which is advantageous for applications where space constraints are a concern. The compact form factor also makes them suitable for integrating small devices and systems.
3. Low Sidelobe Levels: These antennas can be engineered to have low sidelobe levels in their radiation patterns. Low sidelobes help reduce interference from signals from directions other than the main beam, improving the antenna's overall performance.
4. Ease of Integration: Antipodal Vivaldi antennas can be fabricated using microstrip or other planar techniques, making them relatively easy to integrate into printed circuit boards and microwave circuits. This simplifies their integration into various electronic systems.
5. Polarization Flexibility: Depending on the application's specific requirements, they can be designed to support different polarizations, including linear and circular polarizations.

Contribution**:** The proposed antipodal antenna structure makes several significant contributions to the field of antenna technology:

1. Broadband Efficiency: By using the antipodal geometry, the antenna achieves high radiation efficiency over a wide range of frequencies, addressing the research gap of efficient broadband antennas.
2. Miniaturization: The compact design of the antipodal antenna structure allows for integration into small form-factor devices, enabling wireless connectivity in space-constrained environments.
3. Adaptability: The antenna's ability to support multiple frequency bands and communication standards contributes to its versatility, accommodating the evolving needs of wireless technology.
4. Cost-Effectiveness: The design's simplicity and manufacturability contribute to cost-effective production, making it a viable option for mass deployment.

Application (Energy Harvesting): Antennas operating within the frequency range of 30 GHz to 300 GHz, commonly known as the millimeter-wave band, play a crucial role in energy harvesting applications. The high frequencies in this spectrum enable the design of compact and directional antennas, making them suitable for space-constrained environments and applications where precise targeting is essential. One key advantage lies in the increased bandwidth offered by the millimetre-wave range, facilitating the efficient capture of electromagnetic waves for energy harvesting purposes. Furthermore, the atmospheric absorption characteristics at these frequencies can be leveraged to enhance the performance of energy harvesting systems by minimizing interference. Specialized antennas can capture ambient millimeter-wave radiation, such as that from the sun, and rectenna technology, which combines antennas with rectifiers, enables the conversion of these signals into usable electrical energy. These advancements make millimeter-wave antennas integral to developing efficient and compact energy harvesting solutions, with potential applications ranging from wireless sensors to short-range wireless power transmission systems [22],[23].

Novelty/ Originality: The proposed antenna operating within the frequency range of 30 GHz to 300 GHz exhibits a remarkable novelty in its design. With a gain of 12.5 dBi, the antenna demonstrates a heightened capability to focus and amplify signals within the millimeter-wave spectrum. Notably, its low cross-polarization ensures efficient signal purity by minimizing interference from orthogonal polarization components. Moreover, the antenna achieves a high Side Lobe Level (SLL), showcasing an innovative approach to control radiation patterns, enhancing directivity, and mitigating unwanted signal radiation in the surrounding space. This novel design contributes to advancing the performance of antennas in the extremely high-frequency range, making it well-suited for applications requiring precise and directional communication within the millimeter-wave spectrum. This manuscript introduces an asymmetric dual antipodal petunia-shaped antenna for this purpose. In the first section, the focus is on designing a K-band antenna. This involves the creation of patch antennas with various single radiator shapes, including a ball, bulb, axle, and petunia, with a rectangular ground as their base. The second part of the study concentrates on the development of an antenna with a high operating frequency. Here, single-radiator antipodal and dual-radiator antipodal petunia-shaped patches are designed to achieve this objective. In the third section, efforts are directed toward enhancing the antenna's performance by modifying the ground structure. Several ground configurations are explored, including curved, dual-step, symmetric, single-step, and single-step asymmetric grounds. These modifications improve the antenna's high-frequency operation while maintaining the previously achieved lower working frequencies. The final section of the manuscript primarily focuses on the utilization of particle swarm optimization (PSO) to achieve a working frequency range of 30 GHz to 300 GHz. This broad frequency coverage positions the antenna as an ideal candidate for millimeter-wave energy harvesting systems, offering broad signal availability and comprehensive support for millimeter-wave wireless communication systems. It's worth noting that due to the unavailability or limited access to measurement facilities beyond 65 GHz, the manuscript presents measurement results up to 65 GHz. Computer-aided design (CAD) software and simulation tools were used to model, optimize, and fine-tune the proposed antenna's performance, and accordingly, the RLC circuit of the proposed antenna was designed.

II. Antenna Design

A.Design Of Different Patterns of Single Radiator Antennas for Ku, *K, and Ka-Band Application*

Ku, K, and Ka-Band antennas have garnered significant attention in recent research due to their ability to provide high gain and easily adjustable radiation characteristics. Existing literature has theoretically demonstrated that infinite bandwidth is achievable with the antipodal antenna structure. Previous studies have employed techniques, such as circular, elliptical, or Gaussian tapered slot loads, comb-shaped slits, and windmill or fan-shaped designs, to create compact antennas with improved impedance bandwidth and gain.

This manuscript introduces a novel dual radiator antipodal petunia-shaped antenna with an asymmetrical ground structure. We have explored different microstrip circular patch antenna evolutions to realise this innovative structure, as illustrated in Fig. 1. In Fig. 1(a), we have Antenna-I, a circular patch radiator designed on the upper side of the yellow substrate. The lower side of the substrate, depicted in orange, features a partial rectangular ground plane. Antenna-I is subsequently transformed into Antenna-II, which exhibits a tapering bulb-shaped patch structure, as shown in Fig. 1(b). This tapering is executed following a radiation-inspired approach. By implementing this modification, the current path is significantly extended, enhancing the electrical path length of the patch. Consequently, Fig. 2 illustrates a shift in the resonant frequency from 34 GHz to 32 GHz compared to the circular patch antenna. Antenna-II exhibits a broadside radiation characteristic, displaying a monopole-like nature akin to Antenna-I, primarily radiating in the broadside direction.

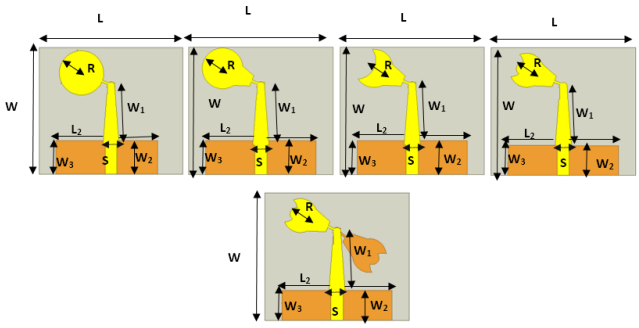

Fig.1. (a) The Antenna I: Ball-shaped single radiator patch, (b) Antenna II: Bulb-shaped single radiator patch, (c) Antenna III: Axle-shaped single radiator patch, (d) Antenna IV: Petunia-shaped single radiator patch, (e) Antenna-V: Antipodal Petunia single radiator antenna

Moreover, Antenna-II undergoes further modification as its etching is altered to assume an axle-shaped structure, resulting in Antenna-III, with a working frequency spanning from 18 GHz to 40 GHz. The tapered curve of the axle-shaped structure contributes to an expanded working bandwidth. Subsequently, the axle-shaped design is refined into a petunia-shaped single radiating patch, designated as Antenna-IV. This configuration provides an operating frequency at the lower end of the spectrum, ranging from 12 GHz to 40 GHz. This frequency range effectively covers the Ku, K, and Ka-bands. It's worth noting that the initial design featured a ball-shaped patch chosen for its curved and tapered characteristics, which are conducive to achieving a high-frequency band [15]. Throughout these designs, the ground structure remains rectangular in all cases. The mathematical equations (1), (2), and (3) used to design Antenna-I, Antenna-II, Antenna-III, and Antenna-IV. The antenna is designed using the circular patch equations, ground plane equations, feedline equations and tapered section equations as discussed below [1],[2],[24].

2.1 Design equation of the Circular patch

The initial step in this process involves adjusting the width of the antenna patch by modifying its specific height or

compactness. The calculation of the subsequent mathematical statement follows this adjustment.

Width calculation-

$$a = \frac{F}{\left[1 + \frac{2h}{\pi F \varepsilon_r}\left(\ln\left\{\frac{\pi F}{2h}\right\} + 1.7726\right)\right]^{0.5}}$$

$$F = \frac{8.791 \times 10^9}{f_r \sqrt{\varepsilon_r}}$$

$\varepsilon_r =$ Dielectric constant of substrate (1)

$$L = 2 \times 2a \quad (2)$$

$$W = 2 \times 2a \quad (3)$$

Where, L and W are the length and width of a substrate used to design a circular patch, *c* is the light velocity, = ϵr is dielectric constant, f_r is resonance frequency.

2.2 Design equations of the ground plane-

Length of ground plane (L_2)

$$L_2 \geq \left(\frac{\lambda_{eff}}{4}\right) \times 2 + L \quad (4)$$

Width of ground plane (w_3)

$$W_3 \geq \left(\frac{\lambda_{eff}}{4}\right) \times 2 + W \quad (5)$$

2.3 Design equations of the feedline

$$Z_T = \frac{60}{\sqrt{\varepsilon_r}} \ln\left(\frac{8d}{W_2} + \frac{W}{4d}\right) \quad (6)$$

$$S = \frac{\lambda}{4} = \frac{\lambda_o}{4\sqrt{\varepsilon_{reff}}} \quad (7)$$

2.4 Design equations of tapered section

$$W_1 \approx \frac{1}{2} \times \frac{c}{f\sqrt{\epsilon_r}} \quad (8)$$

TABLE 1
DIMENSIONS OF ANTENNA (IN MM)

Antenna	L	L2	W	W_1	W_2	W3	R	S
Ball	30	20	30	8	6.5	5	1.5	1
Bulb	30	20	30	8	6.55	5	1.75	1
Axle	30	20	30	8	6.6	5	2.4	1
Petunia	30	20	30	8	6.65	5	2.5	1

This section is focused on achieving a higher operating frequency. It can be seen in Fig.2(a). Among all the four radiators, the Antenna-IV (petunia-shaped) provides an optimum result of working frequency from 12 GHz to 40 GHz. The radiation pattern (E-Plane and H-Plane) of Antenna-IV for K-Band operation at 12 GHz ,24 GHz and 40 GHz are shown in Fig.2(b) with Cross-polar discrimination (XPD) of -16^0, -18^0 and -20^{0,} respectively. These acceptable bandwidth and radiation pattern results motivated the authors to design the next section of the antenna structure. Table-I shows the dimensions of the antenna.

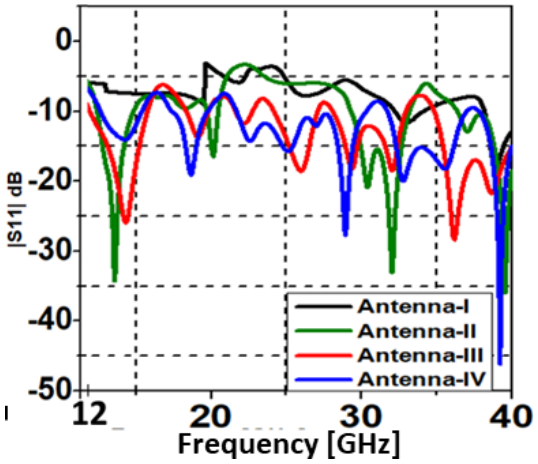

(a)

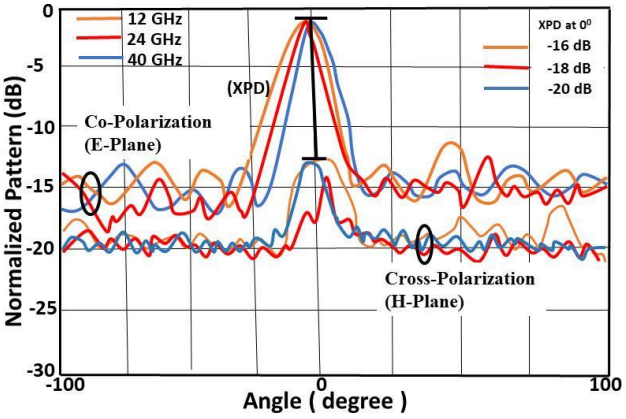

(b)

Fig.2. (a) Comparison of $|S_{11}|$versus frequency graph of Single Radiator Antennas, (b) Radiation pattern (E-Plane and H-Plane) of antenna-IV for K-Bnad

B.Design of a petunia shaped antipodal Single and Dual Radiator antenna

The next design involves an antipodal antenna achieved by relocating the petunia-shaped structure to the opposite side of the dielectric [16]. Consequently, Antenna-IV has been further enhanced to create an antipodal petunia-shaped dual radiator antenna, designated as Antenna-V, as depicted in Fig. 1(e). The antipodal configuration excites higher antenna modes and all the modes featured in the previously designed antennas. An antipodal layout is formed by employing a single patch design on both sides of the dielectric, which contributes to achieving a broadband radiation pattern and associated characteristics.

A dual radiator flower-shaped antipodal antenna, referred to as Antenna-VI, and its prototype is illustrated in Fig. 3(a). The antenna's dimensions consist of a width (W) and length (L) of 30mm each. The petunia structure's outer radius (R) measures 2.5mm, while the inner radius (R1) measures 1.3mm. The

ground structure's dimensions are a length (L2) of 20mm and a width (W3) of 8mm. A tapering line with a width (W1) of 12mm and W2 of 5mm is incorporated into the patch, superimposing the ground structure. The curve mentioned in Fig. 3(a) aids in achieving a higher operating frequency. The angle between the two petunia radiators on the patch is 15 degrees. The proposed antenna is designed with an antipodal structure, enhancing bandwidth.

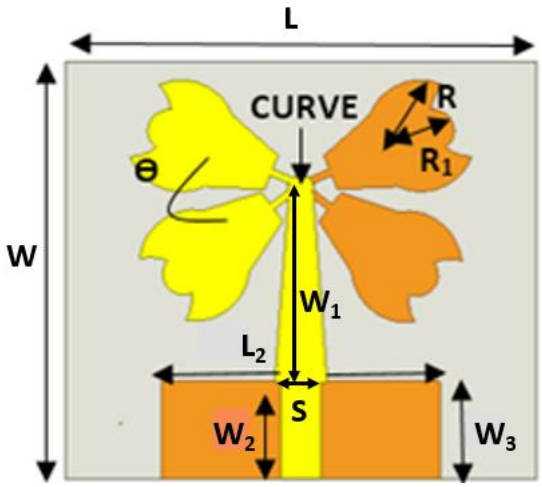

(a)

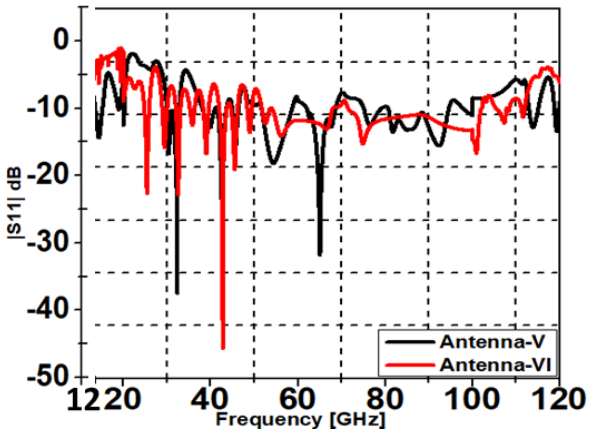

(b)

Fig.3. (a) Antenna VI- Petunia Shaped Antipodal Dual Radiator antenna and the prototype, (b) Comparison of Plot of $|S_{11}|$ versus Frequency graph of Antenna-V and Antenna-VI

In Fig. 3(b), a comparison is presented between the reflection coefficient and frequency for both an antipodal single radiator (Antenna-V) and a dual radiator petunia-shaped patch (Antenna-VI). The graph illustrates that the single antipodal radiator operates effectively within a frequency range of 30 GHz to over 100 GHz. The dual antipodal radiator covers a frequency range from 28 GHz to over 100 GHz. In all cases, the ground structure is rectangular. The tapering implemented in these antennas is aligned with the radiation contour of the antenna structure, thereby proposing a design inspired by radiation patterns.

C. Ground plane modifications for performance enhancement

Modifying the current distribution pattern and enhancing bandwidth are achieved by designing slots on the ground plane. This approach aligns with Babinet's principle in antenna structure, where the slot contour on the ground plane exhibits high impedance. At the same time, the load maintains an input impedance similar to the characteristic impedance (in this case, 50 ohms). The dual antipodal radiator structure (Antenna-VI) is selected as the antenna design, as it yields optimal results among all the compared designs.

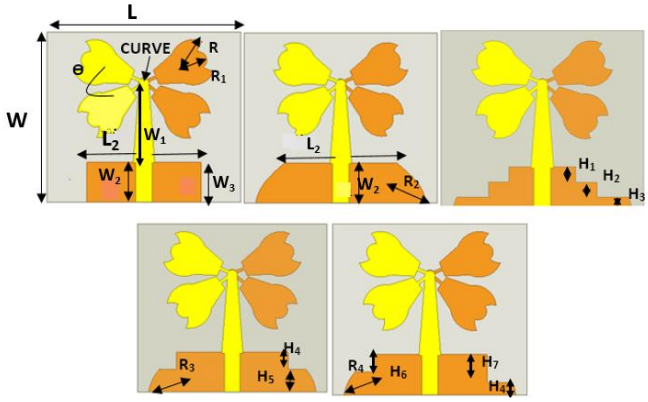

Fig.4. (a) Antenna VI: Rectangular Ground, (b) Antenna VII: Curved Ground, (c) Antenna VIII: Dual step Ground, (d) Antenna IX: Single Step Symmetric Ground, (e)Antenna X: Single Step Asymmetric Ground

The dimensions of the patch remain consistent with the discussion above, with the modifications now focused on the ground plane. The dimensions of the modified ground plane are illustrated in Fig. 4. Specifically, L2 measures 20mm, W1 is 12mm, W2 is 5mm, and W3 is 8mm. Additionally, R2 is 2.5mm, H1 is 4mm, H2 is 2.5mm, H3 is 1.5mm, R3 is 0.3mm, H4 is 2.5mm, H5 is 5.5mm, R4 is 0.8mm, H6 is 5mm, H7 is 6mm, and H8 is 2mm. The comparison of the ground plane is based on these dimensions. The achievement of a more considerable bandwidth results from an improvement in the input impedance matching of the antenna. Instead of a conventional rectangular ground design, a curved ground structure (Antenna VII) is introduced to facilitate smooth current flow, as depicted in Fig. 4. In this representation, the yellow petunia design represents the patch, while the orange design signifies the ground. For the modal analysis of the ground plane-modified antennas, the Eigenmode solver in CST Microwave Studio (MWS) software is utilized. The E-field distribution of Antenna VII is examined, revealing the dominant mode TE13 at 52 GHz, as shown in Fig. 5(a). Additionally, TE32 at 120 GHz and TE23 at 270 GHz are higher modes propagating within the curved ground structure. The resonance of Antenna VII at 52 GHz, as evidenced by the reflection coefficient versus frequency graph, is attributed to the TE13 mode. Fig. 6 illustrates the operational frequency range of Antenna VII (Curved ground), which spans from 52 GHz to 270 GHz.

Antenna VII is further modified into a dual-step ground antenna (Antenna VIII), as depicted in Fig. 4(c). To improve impedance matching, the antenna is designed with a tapered

structure and slots cut in a step-like manner along the feed line. This design extends the electrical length of the patch and provides multiple current paths. Consequently, a shift in resonating frequency from 52 GHz to 48 GHz is observed. Antenna VIII retains all the dominant modes present in Antenna VII and also introduces several new modes, such as TE12 at 48 GHz, TE41 at 88.2 GHz, TE42 at 97.6 GHz, and TE14 at 98.3 GHz, as shown in Fig. 5(b). The operating frequency range of Antenna VIII is verified to be from 46 GHz to 267 GHz, as depicted in Fig. 6.

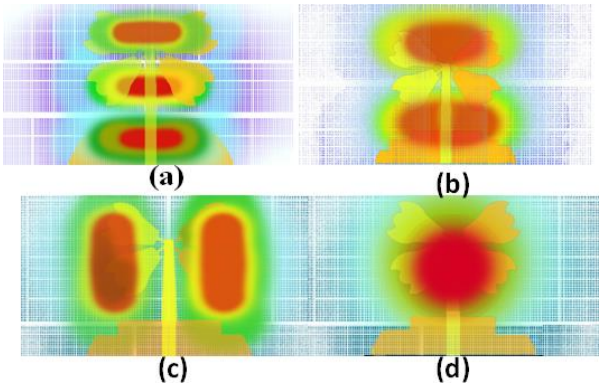

Fig. 5. Dominant mode E-field distribution of Modified ground: (a) TE13 at 52 GHz for Antenna-VII, (b) TE12 at 46.4 GHz for Antenna-VIII, (c) TE21 at 37.8 GHz for Antenna-IX, (d) TE11 at 28.1 GHz for Antenna- X

Next, the single-step symmetric ground structure is designed and upgraded to Antenna IX by tapering and slot cutting, as shown in Fig. 4(c), and this caused the excitement of TE21 mode at 37.8 GHz shown in Fig. 5(c) with all the other modes present in Antenna VIII. The introduction of the ground design structure enhances the reflection coefficient curve of Antenna IX when compared to Antenna VIII, with resonating frequencies of 37 GHz and 42.7 GHz, respectively, as shown in Fig. 6. Upgrading Antenna IX to feature an asymmetric single-step ground plane (Antenna X) leads to an even better load matching, as illustrated in Fig. 4(e). The |S11| versus frequency graph for Antenna X consistently remains below -10 dB over a more comprehensive frequency range in contrast to Antenna IX, with an operational bandwidth extending from 37.2 GHz to 268.1 GHz, as depicted in Fig. 6. This confirms a proper impedance matching. From Fig. 5(d), it is observed that Antenna X exhibits a TE11 mode at 28.2 GHz and an upper mode, TE24, at 40.46 GHz. The shift in the frequency band from 37 GHz to 28.1 GHz is attributed to the presence of the TE11 mode. Antenna X operates with radiation in the frequency range of 28.1 GHz to 273.2 GHz, as verified in Fig. 6. Each operating mode results in radiation from the ground at its respective frequency, as there is a significant variation in the cut-off frequency range of the operating modes. This suggests that different antenna segments emit radiation at various frequencies even with the antenna's size constant.

In summary, the modified ground structures and antipodal designs have been effectively employed to enable radiation in the higher millimeter-wave range. The substrate used for the entire antenna design is a low-loss Rogers RO4232. Rogers RO4232 is known for its low-loss tangent. Loss tangent (tan δ) measures the material's ability to dissipate energy through heat. A low-loss tangent indicates the material has low dielectric losses, critical at mm-wave frequencies. Rogers RO4232 has a relatively high permittivity, typically around 3.2. The suitability of Rogers RO4232 at mm-wave frequencies is also justified by considering the relationship between the loss tangent and frequency. At higher frequencies, having materials with low-loss tangents becomes more critical. Rogers RO4232 is designed and characterized to perform well at microwave and mm-wave frequencies, aligning with the requirements of these frequency ranges. Rogers RO4232 is engineered to have minimal dispersion effects within its specified frequency range. This means that its electrical properties, including εr and tan δ, remain relatively stable across various frequencies, including mm-wave frequencies. In summary, Rogers RO4232 is suitable for use at mm-wave frequencies due to its low loss tangent, high permittivity, and stable electrical properties across the frequency range. These characteristics enable efficient signal transmission, compact antenna designs, and reliable performance at the demanding mm-wave frequencies commonly used in applications like 5G communication, automotive radar, and high-frequency microwave systems. Table-II shows the effect of modified ground on the working frequency of the antenna.

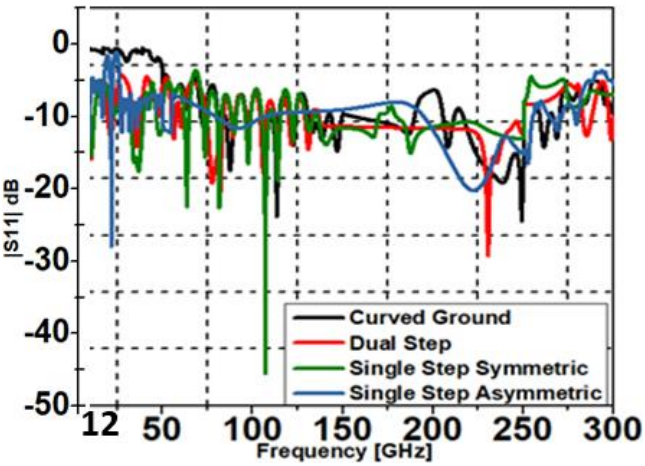

Fig.6. Bandwidth Comparison of Different Ground Modified Antenna Structure

TABLE 2
EFFECT OF MODIFIED GROUND

S. No	Ground	Operating Frequency
1.	Rectangular Ground	28GHz to 112 GHz
2.	Curved Ground	52GHz to 240GHz
3.	Dual-Step Ground	46GHz to 267GHz
4.	Single-Step Symmetric Ground	37.2 GHz to 268.1 GHz
5.	Asymmetric Single Step Ground	28.1GHz to 273.2GHz

III. PSO Optimization of Asymmetric Dual Antipodal Petunia-Shaped Antenna

An antenna is designed to meet specific criteria for return loss and operating frequency, and an optimization process can be employed to achieve these objectives. The antenna configuration is optimized for the desired radiation pattern and return loss. This optimization process involves minimizing the disparity between the actual antenna pattern generated in the simulator and the desired pattern for the antenna. A fitness value is computed by applying different boundary conditions and solving Maxwell's equations, considering both the return loss and radiation pattern characteristics.

To tackle the challenges posed by multimodal effects and significant nonlinearity inherent in full-wave analysis, a Particle Swarm Optimization (PSO) technique is employed as a stochastic global optimizer. PSO aids in finding optimal antenna configurations by iteratively adjusting the design parameters to converge toward the desired performance goals. Mapping the coordinates of each point in the continuous or discrete solution space to a candidate antenna configuration is a crucial aspect of antenna optimization. The utilization of the PSO optimization method for antenna design offers convenience and flexibility for handling both real and binary variables. As evident from Fig. 6, the asymmetric step-ground dual antipodal petunia-shaped antenna demonstrates an optimal bandwidth in the millimeter-wave range. Consequently, to achieve a complete operating millimeter-wave range, Antenna-X is optimised using the PSO algorithm, as outlined in the block diagram presented in Fig. 7.

The operating frequency is closely linked to the length of the current path, so certain geometric parameters, referred to as "swarm" in the context of PSO, are selected based on the simulated current distribution structure in HFSS software. The optimization of the S11 parameter for the petunia design is carried out as a minimax problem. This involves minimizing the relatively poorer S11 value between the two desired frequencies, as determined from the S11 versus frequency graph simulated in HFSS, as shown in Fig. 6. In this case, the lower frequency to be optimized is 28 GHz, and the upper frequency is 273 GHz. The fitness function is decided according to the above-chosen frequency and is given by [17].

$$f = 50 + \max(S11\ [28\ GHz], S11\ [273\ GHz]) \quad (9)$$

From Fig.8, the segment evaluation is done with the swarm initialization and tapered fitness, and accordingly, the different complex equations of a circle, ellipse, and straight lines are used to design the same structure on MATLAB through PSO design code.

$$(z - z_1)(\bar{z} - \bar{z_2}) + (z - z_2)(\bar{z} - \bar{z_1}) = 0 \text{ (For circle slot)} \quad (13)$$

$$r = \frac{a-c}{d-a} = \frac{\sqrt{b^2+c^2}}{d}, d = \frac{a^2}{\sqrt{a^2-b^2}} = \frac{a^2}{c} \text{ and } r = \frac{\sqrt{a^2-b^2}}{a} = \frac{c}{a} \text{ (For ellipse)} \quad (10)$$

$$z = x + iy \text{ (For a straight line)} \quad (11)$$

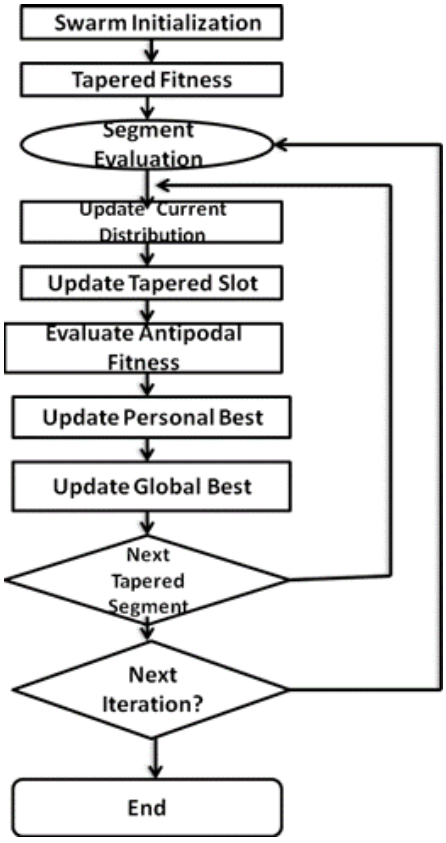

Fig.7. Block Diagram for PSO Optimization

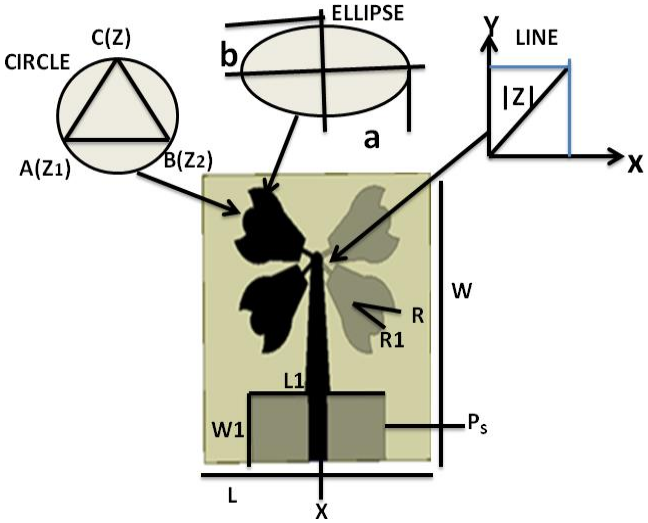

Fig.8. Prototype structure for PSO optimization

Segment evaluation is observed through the current distribution in HFSS design, and the current line and the tapered slot are updated in the MATLAB coding. The value of z_1, z_2, a, b, x, and y from equations (2), (3), and (4) is taken from the point value of the same structure simulated in the HFSS simulator. After the update, the evaluation of the antipodal fitness is done, which mainly depends on the tapered slot position (Ps) and the slot Radii (R and R1) and is given by

$$f = 50 + \max(Ps\ [\text{slot position}], R\ [\text{Bigger slot radius}], R1\ [\text{smaller slot radius}]). \quad (12)$$

Particles are defined in each swarm. By utilizing the current location, each and every particle tracks its position from the current position to the personal best location (pbest) and the global best location (best). The position personally discovered by a particle for the best objective function (fitness) is called best (personal best), and the tracked location of the best-fit function is determined by the swarm is called gbest (global best). The number of iterations is continued until we achieve the desired result. Eight geometric parameters called swarms are chosen according to the antenna design simulated in HFSS software subjected to (unit: mm), as seen in Fig.8.

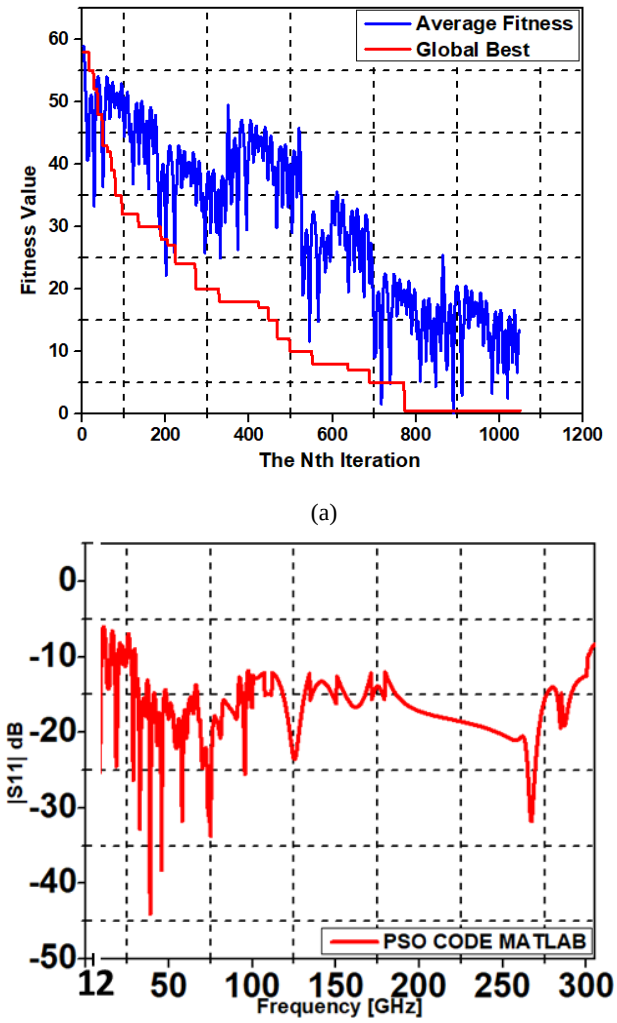

Fig 9. (a) Convergence graph of the PSO by using a 8-segment swarm and total 1000 iterations and applying the fitness function defined in (1), (b) Reflection Coefficient versus frequency graph of PSO MATLAB code

Patch length- L, Patch width-W, Bigger slot radius-R, Smaller slot radius- R1, Slot length- L1, Slot width- W1, Feed position- X and Slot Position- Ps

The boundary condition is as follows-

$$L_1 < L;\ P_S > W_1/2;\ P_S + W_1/2 < W/2;\ |X| < L/2. \quad (13)$$

To maintain the final petunia shape of the antenna and achieve the desired performance within the millimeter-wave band, it is essential to adhere to the above-mentioned boundary conditions for each segment of the antenna design. Before evaluating the fitness function for each iteration, all eight geometric segments undergo scrutiny against the given equations. If any of these equations are not satisfied, the segments are considered to be out-of-boundary. The optimization process for the petunia-shaped antenna structure, as depicted in Fig. 9(a), is carried out over a total of 1000 iterations. The graph is utilized to determine the average fitness and identify the global best, which guides the antenna optimization process. A frequency versus return loss graph is then plotted, demonstrating that the operating frequency spans the entire millimeter-wave band, covering the range from 30 GHz to 300 GHz, as shown in Fig. 9(b).

IV. RLC Circuit of Proposed Antenna Structure

Designing an antipodal antenna using an RLC (Resistance-Inductance-Capacitance) circuit involves several steps [24],[25]. The RLC circuit is used to model the electrical behavior of the antenna, allowing you to optimize its performance.

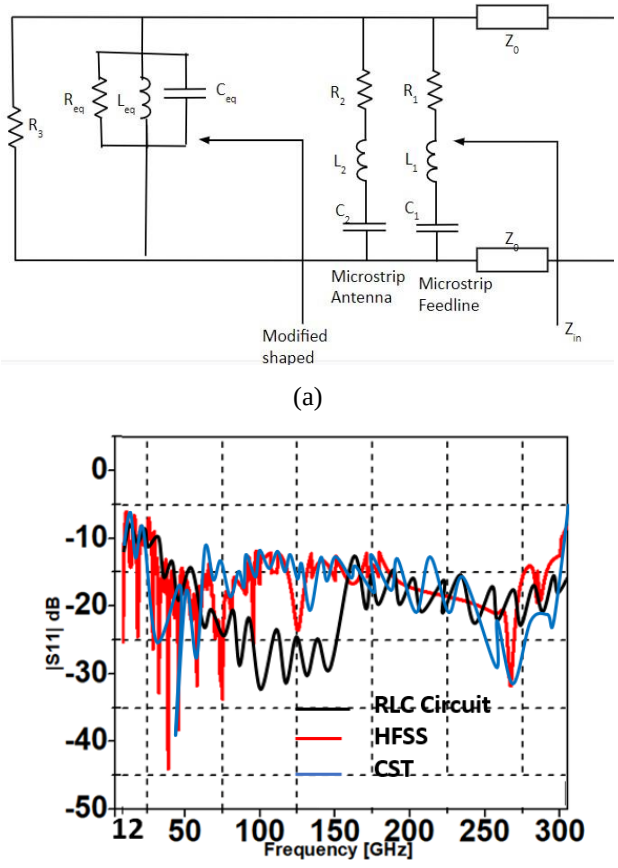

Fig.10. (a) RLC Circuit of the proposed antenna, (b) The comparison graph of reflection coefficient v/s frequency graph of RLC equivalent circuit and HFSS software simulation of the proposed antenna

The lumped component values for the equivalent circuit, specifically R, L, and C, can be initially calculated using Equations (14) – (16), considering the bandwidth and resonant frequency matching to 50 Ω. These values are presented in Table-III. Subsequently, the lumped component values are slightly adjusted using ADS software to achieve the desired characteristics of the Smith chart.

The impedance is modeled by seven parallel RLC cells connected in series, resonating at their respective frequencies. Fig. 10 (b) shows a close alignment between the results derived from HFSS and ADS. Nevertheless, a deviation in the values occurs at higher frequencies due to the approximation of the equivalent circuit model to 50 Ω. As illustrated in the Fig10 (b), a slight discrepancy is observed between the results obtained from the HFSS simulation and ADS.

$$L = \frac{\text{imag}(Z_{11})}{2\pi \cdot f} \tag{14}$$

$$C = \frac{1}{(2\pi \cdot f)^2 L} \tag{15}$$

$$f = \frac{1}{2\pi\sqrt{LC}} \tag{16}$$

TABLE 3
RLC COMPONENT VALUES FOR THE ANTENNA EQUIVALENT CIRCUIT AT 30 GHz.

R_1 (Ω)	R_2 (Ω)	R_3 (Ω)	R_{eq} (Ω)
41.117	38.15	46.57	51.16
C_1 (pF)	C_2 (pF)	Ceq (pF)	Z_0 (Real)
9.8	6.1	12	50
L_1 (pH)	L_2 (pH)	L_{eq} (pH)	Z_0 (Img)
29.9	7.2	110.7	0.1444

This variation can be attributed to adjustments made in the capacitors, inductors, and resistors within the ADS simulation to achieve the desired response, leading to a shift in resonance frequencies compared to the HFSS simulation results. Based on the preceding discussion, it can be concluded that the equivalent circuit model offers valuable insights into the details of resonant frequencies and their significance about the input impedance.

V. FABRICATION AND RESULTS

A. Measurement setup

The investigation of the frequency domain behavior of the antenna is done with the help of a commercial 3D full-wave Electromagnetic simulation and optimization software, Ansys, HFSS, and further validated by another high-performance 3D EM analysis software - CST Studio Suite. Due to constraints in the availability of measurement equipment, a Vector Network Analyzer with a maximum operating frequency of 65 GHz is employed for measuring frequency-dependent parameters such as return loss (VSWR/Impedance). These measurements are conducted using the sweep frequency mode. To measure antenna-related parameters like gain and efficiency, an in-house semi-automated anechoic chamber is utilized. This chamber is equipped with a stepper motor-controlled 2-axis positioner, a standard gain-calibrated broadband antenna, and a power meter. The far-field experimental setup for the proposed antenna structure is illustrated in Fig. 11. In this setup, the antenna under test and a calibrated antenna are positioned approximately 167 cm apart to achieve the required far-field distance within the operating frequency range of 1 GHz to 65 GHz. Typically, a 3.5 mm SMA connector is used in conventional designs for the lower frequency range of operation (DC to 18 GHz). However, for higher working frequencies, a different connector is used. In the case of Antenna-X, the feedline is connected to a PCB female jack connector of 2.92 mm, as shown in Fig. 12.

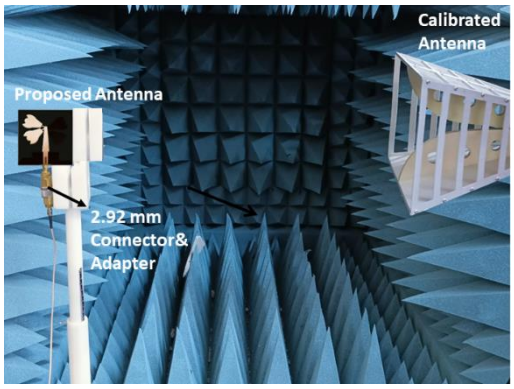

Fig.11. Far-field setup for measurement of Antenna-X

Fig.13 displays the measured return loss, gain, and radiation efficiency of the final version of the proposed antenna structure. The measured gain remains relatively constant across the entire frequency band, ranging from 5.3 dB at 30 GHz to 6 dB at 65 GHz. This consistency is attributed to the measurement conducted in a specific single direction, while the simulated gain accounts for all directions. The measured return loss versus frequency graph for the proposed antenna demonstrates good impedance matching, with S11 consistently below -10 dB within the measured frequency band of 30.25 GHz to 65 GHz. A slight deviation of 250 MHz from the simulated values is observed, likely due to factors such as extra soldering, fabrication or material tolerances, or minor errors during the fabrication process. The measured radiation efficiency of the antenna varies between 89% and 92% across the frequency range from 30 GHz to 65 GHz, indicating that the proposed antenna performs well as a radiator.

Potential applications for the proposed antenna include military and imaging systems, automotive radars, telecommunications, remote sensing, security screening, and energy harvesting technology. Cross-polar discrimination (XPD) of the proposed antenna is simulated at 90 GHz, 180 GHz, and 270 GHz, as shown in Fig. 14(a).

In all cases, the XPD values are below -33 dB, indicating low cross-polarization, which enhances the antenna's overall performance. Fig. 14(b) presents a comparison of the simulated Side Lobe Level (SLL) of the proposed antenna using both HFSS and CST simulations. At 60 GHz, the SLL values are -22 dB and -18 dB for HFSS and CST, respectively. This comparison demonstrates that the proposed antenna offers an ultra-low SLL along with excellent XPD,

highlighting its novelty and performance characteristics. Fig. 15 shows the antenna's radiation pattern at 50 GHz, 150 GHz and 270 GHz.

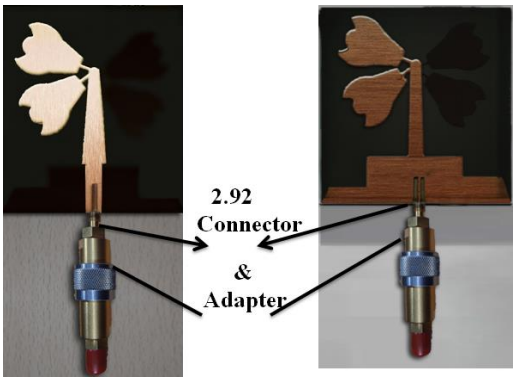

Fig.12. Fabricated patch: (a) (Front) and (b) ground (back) view of prototyped Antenna-X

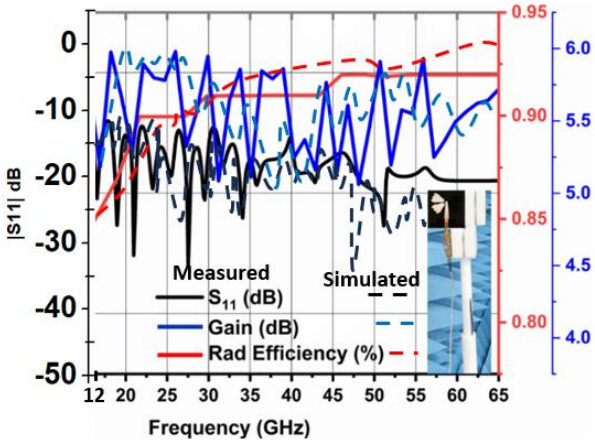

Fig.13. Simulated and measured |S11|, Gain, Radiation efficiency versus frequency (GHz) graph of the Antenna-X

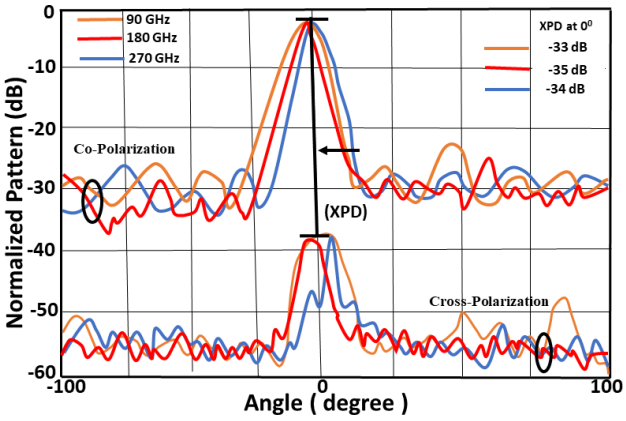

(a)

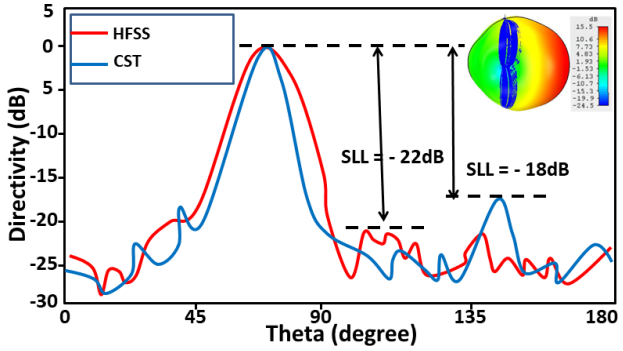

(b)

Fig. 14. (a) Cross-polar discrimination (XPD) of the final structure, (b) Side Lobe Level of the final structure

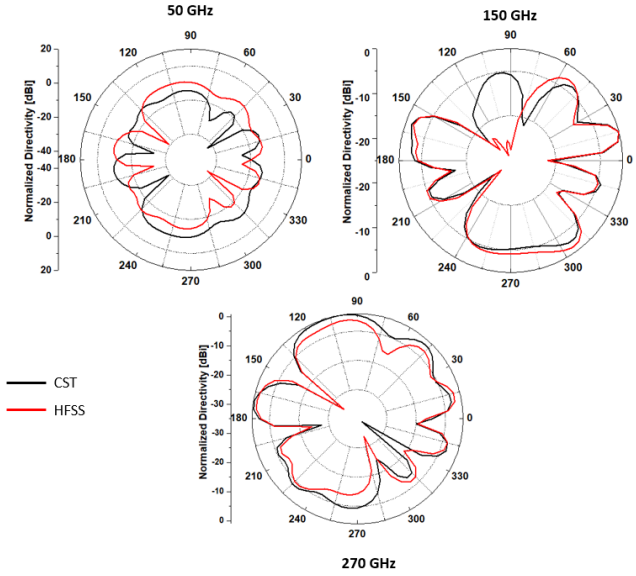

Fig.15. Radiation pattern at 50 GHz, 150 GHz and 270 GHz

VI. Comparison with State-of-Art Work

The proposed work is compared with state-of-the-art research and summarized in Table-IV. Various types of antennas are considered, and the design methodology for achieving broadband performance is outlined. Prior research has primarily focused on designing millimeter-wave antennas for higher operating frequency bands [2,18] or lower frequency bands [19,20]. In contrast, the proposed work offers a distinct advantage as it covers the entire millimeter-wave frequency band. Consequently, this single antenna can be utilized for lower and higher frequency bands. The proposed petunia-shaped asymmetric dual antipodal antenna is a compact design with broadband characteristics, making it a valuable addition to the field. A comparison between the state-of-the-art and proposed antenna designs reveals distinctive features, particularly in the operating frequency range spanning from 30 GHz to 300 GHz. The proposed antenna outperforms existing designs in several key aspects. Its ability to effectively cover the high-frequency spectrum makes it well-suited for applications requiring operation in the millimeter-wave frequency range.

Moreover, the proposed antenna demonstrates superior performance characteristics within its designated frequency band, showcasing advancements in miniaturization, radiation efficiency, and possibly other relevant parameters. This comparative analysis highlights the innovative contributions of the proposed antenna in pushing the boundaries of antenna technology within the specified frequency range.

VII. CONCLUSION

In conclusion, the development of millimeter-wave antennas, particularly the petunia-shaped asymmetric dual antipodal antenna presented in this work, offers a significant advantage in achieving broadband performance. This antenna design covers the entire millimeter-wave frequency band, bridging the gap between lower and higher frequency applications. Its compact form factor and broadband characteristics make it a versatile solution for various sectors, including military and imaging systems, automotive radar, telecommunications, remote sensing, security screening, and energy harvesting technology. As the demand for high-frequency communication and sensing systems continues to grow, millimeter-wave antennas like the one proposed here will play a crucial role in advancing the capabilities and efficiency of these technologies, paving the way for a more connected and data-rich future. The antenna size is 30*30 mm^2 with a peak gain of 6 dBi and radiation efficiency of 89-92% in the entire mm-wave band. The 30 mm size of the antenna is a deliberate design choice to accommodate the short wavelengths characteristic of millimeter-wave frequencies, ensuring effective signal capture and transmission within the specified frequency range. This compatibility between antenna size and millimeter-wave frequencies is crucial for achieving the desired gain, low cross-polarization, and high SLL, making the proposed antenna well-suited for applications in advanced communication systems operating in the millimeter-wave spectrum.The proposed antenna offers a complete millimeter wave frequency band, i.e., from 30 GHz to 300 GHz, with ultra-low SLL with good XPD, highlighting the structure's novelty. A measurement facility (anechoic chamber with frequency-dependent absorbers) beyond 65 GHz is not available/accessible to the authors, so the measurement up to 65 GHz is shown in the manuscript.

TABLE 4
COMPARISON OF STATE-OF-ART WORK AND PROPOSED WORK

Ref and Year	Size (L×W in mm^2) and % Miniaturized Dimension(λ_{mm})	B.W (GHz)	Substrate	Gain	Complexity	Practical Use / Utilization at the mm-wave frequencies
[15] and 2021	14.7×11.9 and 5%	55-65	ROGERS CuClad 217	3 dBi	Complex	Internet-of-Things systems.
[16] and 2020	9×5 and 11.11%	23.41-33.92	Rogers RT Duroid 5880	10.7 dBi	Complex	Gbps 5G
[17] and 2023	5×5 and 9%	24-40	Multilayer	4 dBi	Simple	Antenna-in-package (AiP)
[18] and 2021	20×8 and 3.84%	75- 80	-	17 dBi	Complex	Imaging system
[19] and 2021	10×3.5 and 10.71% / 7.89%	28/ 38	Rogers RT Duroid 5880	8.7 dBi	Complex	Beam Steering in 5G
[20] and 2021	50×40 and 4%	55-95	Rogers RT Duroid 5880	7 dBi	Simple	5G and mm-wave
[21] and 2021	12.8× 10.87 and 5%	58.46 to 62.14	Isola Tachyon	10 dBi	Complex	Antenna-in-package (AiP)
This work	30×30 and 16%	30-300	Rogers RO4232	6 dBi	Simple	Energy Harvest

VIII. DECLARATIONS

A. Funding: No funds, grants, or other support was received by the authors.

B. Competing Interest: The authors have no relevant financial or non-financial interests to disclose.

REFERENCES

[1] Balanis, C. A., *Antenna Theory Analysis and Design. 2nd edition*, USA: John Wiley and Sons, 2009.

[2] M. Singh, A. Basu and S. K. Koul, "Circular Patch Antenna with Quarter Wave Transformer Feed for Wireless Communication," *Annual IEEE India Conference*, New Delhi, India, pp. 1-5, 2006.

[3] Sneha Tiwari and Srikanta Pal, "Tapered-Slot Radiation-Traveling Wave Mechanism Inspired Extreme Wideband Efficient Antenna with Ultra-Low SLL," in *Electromagnetics*, vol. 43, no. 8, pp. 591-606, 2023.

[4] M. -C. Tang, X. Chen, M. Li and R. W. Ziolkowski, "Particle Swarm Optimized, 3-D-Printed, Wideband, Compact Hemispherical Antenna," in *IEEE Antennas and Wireless Propagation Letters*, vol. 17, no. 11, pp. 2031-2035, Nov. 2018.

[5] H. S. Girija, R. Sudhakar, K. M. Abdul Kadhar, T. S. Priya, S. Ramanathan and G. Anand, "PSO Based Microstrip Patch Antenna Design for ISM Band" *2020 6th International Conference on Advanced Computing and Communication Systems (ICACCS)*, Coimbatore, India, pp. 1209-1214, 2020.

[6] M. -S. Kang, Y. -J. Won, B. -G. Lim and K. -T. Kim, "Efficient Synthesis of Antenna Pattern Using Improved PSO for Spaceborne SAR Performance and Imaging in Presence of Element Failure," in *IEEE Sensors Journal*, vol. 18, no. 16, pp. 6576-6587, 2018.

[7] M. Alibakhshikenari *et al*., "A Comprehensive Survey on Antennas On-Chip Based on Metamaterial, Metasurface, and Substrate Integrated Waveguide Principles for Millimeter-Waves and Terahertz Integrated Circuits and Systems," in *IEEE Access*, vol. 10, pp. 3668-3692, 2022.

[8] M. Alibakhshikenari, B.S. Virdee, A.A. Althuwayb; D. Mariyanayagam, E. Limiti, "Compact and Low-Profile On-Chip Antenna Using Underside Electromagnetic Coupling Mechanism for Terahertz Front-End Transceivers". *Electronics*, vol. 10, 2021

[9] A.A Althuwayb, M. Alibakhshikenari, B.S. Virdee, H. Benetatos, F. Falcone, E. Limiti, "Antenna on Chip (AoC) Design Using Metasurface and SIW Technologies for THz Wireless Applications," *Electronics*, vol.10, 2021.

[10] M. Alibakhshikenari, B.S. Virdee, S. Salekzamankhani, *et al*."High-Isolation Antenna Array using SIW and Realized with a Graphene Layer for Sub-Terahertz Wireless Applications" *Scientific Reports* vol. 11, 2021.

[11] M. Alibakhshikenari, B.S. Virdee, A.A. Althuwayb *et al.*"Study on on-Chip Antenna Design Based on Metamaterial-Inspired and Substrate-Integrated Waveguide Properties for Millimetre-Wave and THz Integrated-Circuit Applications," *Journal of Infrared, Milliter and Terahertz Waves*, vol. 42, pp. 17–28, 2021.

[12] M. Alibakhshikenari, B.S. Virdee, C.H. See *et al.*"Study on Improvement of the Performance Parameters of a Novel 0.41–0.47 THz On-Chip Antenna Based on Metasurface Concept Realized on 50 μm GaAs-layer," *Scientific Reports*, vol. 10, 2020.

[13] M. Alibakhshikenari, B.S. Virdee, C.H. See *et al.*"High-Gain Metasurface in Polyimide On-Chip Antenna Based on CRLH-TL for Sub-Terahertz Integrated Circuits," *Scientific Reports*, vol. 10, 2020.

[14] M.N.E. Temmar, A. Hocini, Dj. Khedrouche, M. Zamani. "Analysis and Design of a Terahertz Microstrip Antenna Based on a Synthesized Photonic Bandgap Substrate using BPSO" *Journal of Computational Electronics*, vol. 18, pp. 231–240, 2019.

[15] K. Trzebiatowski, M. Rzymowski, L. Kulas and K. Nyka, "Simple 60 GHz Switched Beam Antenna for 5G Millimeter-Wave Applications," in *IEEE Antennas and Wireless Propagation Letters*, vol. 20, no. 1, pp. 38-42, Jan. 2021.

[16] H. Ullah and F. A. Tahir, "A High Gain and Wideband Narrow-Beam Antenna for 5G Millimeter-Wave Applications," in *IEEE Access*, vol. 8, pp. 29430-29434, 2020.

[17] Z. Siddiqui *et al*., "Dual-Band Dual-Polarized Planar Antenna for 5G Millimeter-Wave Antenna-in-Package Applications," in *IEEE Transactions on Antennas and Propagation*, vol. 71, no. 4, pp. 2908-2921, April 2023.

[18] Z. Chen, P. Teng and J. Wang, "An E-Band Beam Sharpening Antenna Based on Monopulse Comparator," in *IEEE Access*, vol. 9, pp. 73262-73270, 2021.

[19] A. M. Montaser and K. R. Mahmoud, "Deep Learning Based Antenna Design and Beam-Steering Capabilities for Millimeter-Wave Applications" in *IEEE Access*, vol. 9, pp. 145583-145591, 2021.

[20] S. Y. A. Fatah, E. K. I. K. I. Hamad, W. Swelam, A. M. M. A. Allam, M. F. Abo Sree and H. A. Mohamed, "Design and Implementation of UWB Slot-Loaded Printed Antenna for Microwave and Millimeter Wave Applications," in *IEEE Access*, vol. 9, pp. 29555-29564, 2021.

[21] S. R. Govindarajulu, R. Hokayem and E. A. Alwan, "A 60 GHz Millimeter-Wave Antenna Array for 3D Antenna-in-Package Applications," in *IEEE Access*, vol. 9, pp. 143307-143314, 2021.

[22] M. A. Ullah, R. Keshavarz, M. Abolhasan, J. Lipman, K. P. Esselle and N. Shariati, "A Review on Antenna Technologies for Ambient RF Energy Harvesting and Wireless Power Transfer: Designs, Challenges and Applications," in *IEEE Access*, vol. 10, pp. 17231-17267, 2022.

[23] Atul Varshney, Nishigandha Cholake and Vipul Sharma "Low-Cost ELC-UWB Fan-Shaped Antenna Using Parasitic SRR Triplet for ISM Band and PCS Applications," *International Journal of Electronics Letters*, vol. 10, pp. 391-402, 2021.

[24] Atul Varshney, Vipul Sharma and A.K. Sharma "RLC-equivalent Circuit based Stub Loaded 2x2 MIMO Antenna for Wireless Applications," vol. 29.pp. 44-54, 2023.

[25] Atul Varshney and Vipul Sharma "Aerodynamic slotted SIW-to-MS line transition using mitered end taper for satellite and RADAR communications." *World Journal of Engineering*, vol. 21, pp. 588-603, 2024.